Solar Phys
DOI 10.1007/s11207-013-0466-6

Dependence of Geomagnetic Storms on Their Associated Halo CME Parameters

Jae-Ok Lee · Y.-J. Moon · Kyoung-Sun Lee · R.-S. Kim

Received: 18 December 2011 / Accepted: 20 December 2013

Abstract We compare the geoeffective parameters of halo coronal mass ejections (CMEs). We consider 50 front-side full-halo CMEs (FFH CMEs), which are from the list of Michalek, Gopalswamy, and Yashiro (*Solar Phys.* **246**, 399, 2007), whose asymmetric-cone model parameters and earthward-direction parameter were available. For each CME we use its projected velocity [V_p], radial velocity [V_r], angle between cone axis and sky plane [γ] from the cone model, earthward-direction parameter [D], source longitude [L], and magnetic-field orientation [M] of its CME source region. We make a simple linear-regression analysis to find out the relationship between CME parameters and Dst index. The main results are as follows: i) The combined parameters [$(V_r D)^{1/2}$ and $V_r\gamma$] have higher correlation coefficients [cc] with the Dst index than the other parameters [V_p and V_r]: cc = 0.76 for $(V_r D)^{1/2}$, cc = 0.70 for $V_r\gamma$, cc = 0.55 for V_r, and cc = 0.17 for V_p. ii) Correlation coefficients between $V_r\gamma$ and Dst index depend on L and M; cc = 0.59 for 21 eastern events [E], cc = 0.80 for 29 western events [W], cc = 0.49 for 17 northward magnetic-field events [N], and cc = 0.69 for 33 southward magnetic-field events [S]. iii) Super geomagnetic storms (Dst ≤ -200 nT) only appear in the western and southward magnetic-field events. The mean absolute Dst values of geomagnetic storms (Dst ≤ -50 nT) increase with an order of E + N, E + S, W + N, and W + S events; the mean absolute Dst value (169 nT) of W + S events is significantly larger than that (75 nT) of E + N events. Our results demonstrate

J.-O. Lee · Y.-J. Moon (✉)
School of Space Research, Kyung Hee University, Yongin, Korea
e-mail: moonyj@khu.ac.kr

J.-O. Lee
e-mail: ljoking@khu.ac.kr

Y.-J. Moon
Astronomy and Space Science, Kyung Hee University, Yongin, Korea

K.-S. Lee
Institute of Space and Astronautical Science, Japan Aerospace Exploration Agency, Sagamihara, Japan

R.-S. Kim
Korea Astronomy and Space Science Institute, Daejeon, Korea

Published online: 24 January 2014

that not only do the cone-model parameters together with the earthward-direction parameter improve the relationship between CME parameters and Dst index, but also the longitude and the magnetic-field orientation of a FFH CME source region play a significant role in predicting geomagnetic storms.

Keywords Coronal mass ejection, initiation and propagation · Magnetosphere, geomagnetic disturbances

1. Introduction

Coronal mass ejections (CMEs) are giant magnetized bubbles that are ejected from the lower corona of the Sun. CMEs and their associated shocks are thought to be key drivers of space weather as they can cause geomagnetic storms (Gosling *et al.*, 1991; Brueckner *et al.*, 1998).

Several CME parameters have been proposed to explain the geoeffectiveness of CMEs (Wang *et al.*, 2002; Srivastava and Venkatakrishnan, 2004; Kim *et al.*, 2005; Moon *et al.*, 2005; Michalek *et al.*, 2006; Song *et al.*, 2006; Michalek, Gopalswamy, and Yashiro, 2007). The angular width of a halo CME is an important geoeffective parameter. Several researchers have found that front-side full-halo CMEs (FFH CMEs) are more strongly related to geomagnetic storms than front-side partial-halo CMEs (FPH CMEs) (Wang *et al.*, 2002; Zhang *et al.*, 2003; Zhao and Webb, 2003). Zhang *et al.* (2007) reported that among the 68 identified CMEs associated with major geomagnetic storms (Dst ≤ -100 nT), 46 CMEs (68 %) were FFH CMEs and 22 CMEs (32 %) were FPH CMEs.

The velocity of a CME is also an important geoeffective parameter. Several studies reported that projected CME velocities [V_{p}] obtained by a linear fit to height–time measurements in the *Large Angle and Spectrometric Coronagraph* (LASCO: Brueckner *et al.*, 1995), which is onboard the *Solar and Heliospheric Observation* (SOHO), field of view, were roughly correlated with the Dst indices (Srivastava and Venkatakrishnan, 2004). Radial velocities [V_{r}] from the cone model (Michalek, Gopalswamy, and Yashiro, 2003) were also roughly correlated with the Dst indices (Michalek *et al.*, 2006). Michalek, Gopalswamy, and Yashiro (2007) showed that the V_{r} angle between cone axis and sky plane [γ] derived from the asymmetric-cone model (Michalek, 2006) has a higher correlation coefficient (cc = 0.74) with the Dst index than the value of $V_{\mathrm{p}}\gamma$ obtained from the SOHO/LASCO CME catalog.

Another important geoeffective parameter is the earthward-direction parameter [D], defined as the ratio of the shorter distance to the longer distance of the CME front edge measured from the solar center along the line which passes through both the centers of the ellipse and the Sun (Figure 1 of Moon *et al.*, 2005). If a CME originates from the front side of the Sun, this parameter implies whether the CME can propagate toward the Earth or not. Kim *et al.* (2008) have investigated the relationship between the earthward-direction parameter and Dst index. They demonstrated that CMEs with large earthward-direction parameters ($D \geq 0.4$) are highly associated with geomagnetic storms and all CMEs with super geomagnetic storms (Dst ≤ -200 nT) have direction parameters larger than 0.6.

In addition, the longitude and the magnetic-field orientation of a CME source region are important geoeffective parameters. Several studies found that the disk CMEs are more geoeffective than limb CMEs (Wang *et al.*, 2002; Kim *et al.*, 2005; Gopalswamy *et al.*, 2007; Zhang *et al.*, 2007), and many storm sources originate from the western hemisphere rather than the eastern hemisphere (Wang *et al.*, 2002; Zhang *et al.*, 2007). Michalek *et al.* (2006) observed that only CMEs occurring in the western hemisphere cause severe geomagnetic

storms (Dst ≤ -150 nT). Several researchers have studied the geoeffectiveness depending on the magnetic-field orientation of a CME source region (Pevtsov and Canfield, 2001; Kang *et al.*, 2006; Song *et al.*, 2006). Song *et al.* (2006) determined magnetic-field orientations by using a potential-field model (Abramenko, 1986). They showed that 92 % (11/12) of the CME source regions associated with super geomagnetic storms (Dst ≤ -200 nT) and 73 % (22/30) of the CME source regions associated with intense geomagnetic storms (Dst ≤ -100 nT) had southward magnetic-field orientations.

Although many studies have been carried out on the relationship between CME parameters and geomagnetic storms, we do not know which CME parameter is the best proxy related to geomagnetic storms. The purpose of this article is to find the best proxy, one CME parameter or its combinations, for geomagnetic storms and the dependence of geomagnetic storms on their associated CME parameters. For this we use 50 FFH CMEs from 2001 to 2002 and geomagnetic disturbances related to these events, which are from the list of Michalek, Gopalswamy, and Yashiro (2007).

The article is organized as follows: In Section 2, we describe the data and analysis. Results and discussion are given in Section 3. A brief summary and our conclusion are presented in Section 4.

2. Data and Analysis

2.1. Data

We use CME parameters and their associated Dst data from Table 1 of Michalek, Gopalswamy, and Yashiro (2007). This table consists of observed dates of 69 FFH CMEs using SOHO/LASCO-C2, projected CME velocities, CME parameters derived from the asymmetric-cone model (Michalek, 2006) such as radial velocities [V_r] and the angles between cone axis and sky plane [γ] of the CMEs, Dst indices obtained from the World Data Center (wdc.kugi.kyoto-u.ac.jp), and travel times. In this study, we only consider 50 FFH CMEs related to geomagnetic disturbances (Dst ≤ -18 nT) for investigating the relationship between CME parameters and Dst index. We assume that the uncertainty of the radial velocity is 94 km s^{-1}, which is an average of the root mean square [RMS] errors given by Michalek, Gopalswamy, and Yashiro (2007) who determined the RMS error as the difference between fitted projected speeds and measured projected speeds. According to Gonzalez *et al.* (1994) and Kim *et al.* (2010), we classify geomagnetic storms as follows:

i) moderate geomagnetic storms, minimum Dst falls between -50 and -100 nT;
ii) intense geomagnetic storms, minimum Dst falls between -100 and -200 nT; and
iii) super geomagnetic storms, minimum Dst of -200 nT or less.

In addition, we derive the earthward-direction parameter [D] as a CME parameter for the geo-effectiveness using LASCO images. Figure 1 shows an example to determine the earthward-direction parameter of the CME observed at 22:06 UT on 26 July 2002 by using SOHO/LASCO-C2. The outer white ellipses are plotted by visual inspection of the CME front edges. As exemplified in Figure 1, we determine the earthward-direction parameters for a single CME in LASCO-C2 and C3 fields of view. These two determined values are similar: 0.48 for C2 and 0.41 for C3. For all 50 events, the RMS value of the differences between the earthward-direction parameter from LASCO-C2 and C3 is about 0.15. We use the earthward-direction parameters from the LASCO-C3 images, since they have clearer CME front edges than those from the C2 images, and they give us final information on the

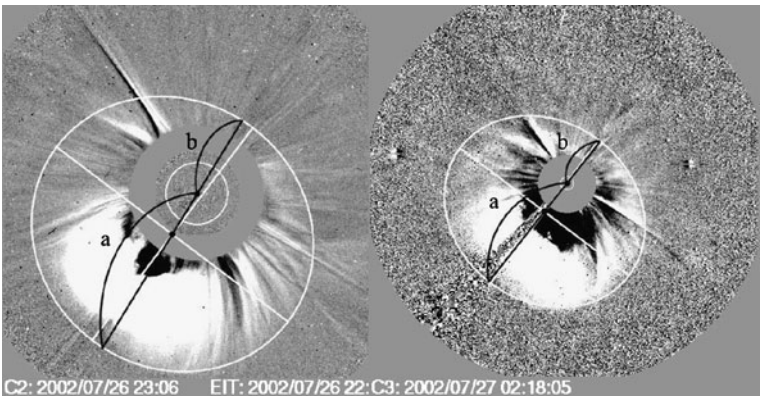

Figure 1 LASCO-C2 (left) and C3 (right) running-difference images to exemplify how to determine the earthward-direction parameter [D], which is defined as the ratio of the shorter distance [b] to the longer distance [a] of the CME front edge measured from the solar center along the black line [b/a]. Note that the line passes both through the centers of the outer white ellipse and the inner white circle. The outer ellipse indicates the CME front edge. The inner circle indicates the location and size of the solar disk (Figure 1 of Kim *et al.*, 2008).

CME propagation in LASCO field of view. If the LASCO-C3 images do not have clearer CME front edges than those from the C2 images, we use LASCO-C2 images. From another perspective, some uncertainty for determining the earthward-direction parameter of a CME may exist because an ellipse is plotted by visual inspection of the CME front edge. To find out the uncertainty of the earthward-direction parameter, we consider three typical CMEs ($D = 0.94$ for the 29 March 2001 CME, $D = 0.41$ for the 26 July 2002 CME, and $D = 0.22$ for the 18 July 2002 CME), which are the maximum, mode, and minimum values of the earthward-direction parameter, respectively. We make ten measurements of the earthward-direction parameter, and then we calculate its standard deviations [sd] for each CME: sd $= 0.036$ for the 29 March 2001 CME, sd $= 0.024$ for the 26 July 2002 CME, and sd $= 0.031$ for the 18 July 2002 CME. For this study, we assume that the uncertainty of the earthward-direction parameter is 0.03, which is an average of these standard deviations. The method to determine this parameter is well described by Moon *et al.* (2005) and Kim *et al.* (2008). If a CME is propagating directly toward the Earth, D is close to unity, and the CME may produce a geomagnetic storm. If a CME is propagating away from the Sun–Earth line, D is close to zero, and the CME may not drive a geomagnetic storm.

To identify the source longitude [L] of a CME, we use the source locations in the flare list compiled by National Geophysical Data Center (NGDC) (ftp.ngdc.noaa.gov/STP/SOLAR_DATA/SOLAR_FLARES/FLARES_XRAY). Among 50 FFH CMEs, 48 FFH CMEs accompany X-ray flares, while 2 FFH CMEs do not accompany X-ray flares and Hα flares. In the case of a flare-associated CME, we assume the location of an X-ray flare as the location of a CME accompanied by an X-ray flare. Otherwise, we carefully look into their SOHO/LASCO images and SOHO/*Extreme ultraviolet Imaging Telescope* (EIT: Delaboudinière *et al.*, 1995) running-difference images. By investigating any disk activity associated with a CME, such as EUV brightening/dimming or flare-associated ejecting loops, we determine the source location of the CME. Figure 2 shows a set of SOHO/LASCO-C2 images and EIT running-difference ones for the 19 March 2001 event, which is not associated with an X-ray flare. As can be seen in Figure 2, we check the EUV brightening within the white square after the CME eruption. We assume the location of an EUV activity associated with a

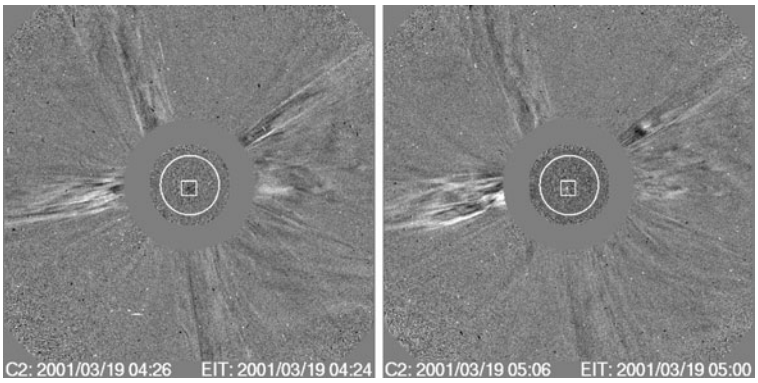

Figure 2 SOHO/LASCO running-difference images (Left: before the event, right: after the event) of a 19 March 2001 CME event with their corresponding SOHO/EIT ones. The white square indicates its source location. The white circle indicates the location and size of the solar disk.

CME is the location of a CME unaccompanied by an X-ray flare. Since the source locations of CMEs without flares are determined by SOHO/EIT images whose pixel size is 2.6 arcsec, their errors should be within a few degrees.

We determine the magnetic-field orientation [M] of a CME source region by applying the potential-field model (Abramenko, 1986) to SOHO/*Michelson Doppler Imager* (MDI: Scherrer *et al.*, 1995) images. If the direction of M is toward the North Pole or South Pole of the Sun, we consider M as the northward or the southward direction, respectively. Among 50 FFH CMEs, 46 FFH CMEs occur near the center of the Sun, 4 FFH CMEs occur near the limb of the Sun. In the case of the center events, we easily determine the directions of magnetic-field orientations by visual inspection of the structures of the field lines. However, in the case of the limb events, we cannot easily determine the directions of magnetic-field orientations because it is hard to discriminate between the main positive polarity regions and the main negative polarity regions by projection effects such as decrease of projected area and the change of magnetic-field strength and polarity. In order to determine the magnetic-field orientations of limb events, we have carefully identified SOHO/MDI magnetograms of the active regions related to four limb events by considering the solar rotation rate. By assuming that their magnetic-field orientations had not been changed during several days, we determine the magnetic-field orientations of these limb events. Since we determined the magnetic-field orientations of 50 FFH CMEs using the Potential-Field Solar Surface [PFSS] model without any difficulty, we think that the uncertainty for determining the magnetic-field orientations of the CME source regions is negligible. Figure 3 shows an example to determine magnetic-field orientations in the source region of the CME observed at 16:50 UT on 19 October 2011 by using SOHO/LASCO-C2.

Table 1 summarizes the information of the 50 front-side full-halo CMEs. The first three columns are from the SOHO/LASCO catalog and give the date of the first appearance in the LASCO field of view, the projected velocities [$V_{\rm p}$], and normalized $V_{\rm p}$ which is defined as the projected velocity divided by the maximum projected velocity. In column 4 the earthward-direction parameters [D] are presented. The radial velocities [$V_{\rm r}$] and parameters [γ] estimated from the asymmetric-cone model are shown in columns 5 and 7, respectively. In columns 6 and 8 the normalized $V_{\rm r}$ and the normalized γ are presented. The source locations and magnetic-field orientations [M] are shown in columns 9 and 10, respectively. In column 11 the minimal values of the Dst indices for geomagnetic disturbances caused by FFH CMEs are presented.

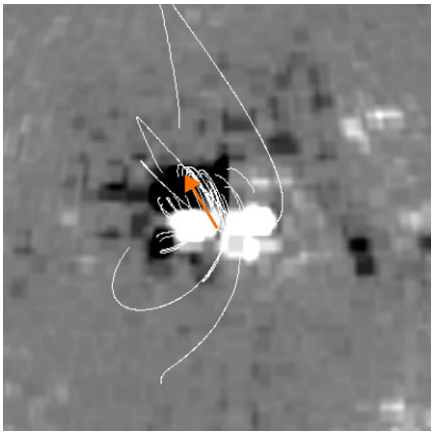

Figure 3 Magnetic-field lines, which are computed from the potential-field approximation, based on SOHO/MDI magnetogram taken at 16:03 UT on 19 October 2001. The orange arrow indicates the direction of the magnetic-field orientation. The field of view is 12×12 arcminutes.

2.2. Analysis

We make a simple linear regression analysis to find the relationship between CME parameters and Dst index. We normalize CME parameters such as $V_{\rm p}$, $V_{\rm r}$, and γ from zero to one for comparing the geoeffectiveness of the CME parameters. Here the geoeffectiveness is indicated by the slope of the linear regression equation for each parameter. For example, we use the normalized $V_{\rm r}$, which is defined as the radial velocity divided by the maximum radial velocity. Normalized CME parameters are shown in columns 3, 6, and 8 of Table 1. We make the same analysis by dividing all CMEs into several sub-groups according to their source longitudes (eastern and western events) and according to their magnetic-field orientations (northward magnetic-field and southward magnetic-field events). We also examine the dependence of the geomagnetic storms on the combination of longitude and magnetic-field orientation such as the following: eastern and northward magnetic-field events [E + N], eastern and southward magnetic-field events [E + S], western and northward magnetic-field events [W + N], and western and southward magnetic-field events [W + S].

3. Results and Discussion

3.1. Comparison of Geoeffective CME Parameters

Figure 4 shows the relationship between the Dst index and the four geoeffective CME parameters: the projected velocity [$V_{\rm p}$], the radial velocity [$V_{\rm r}$], the combined parameter [$V_{\rm r}\gamma$], and the combined parameter [$(V_{\rm r}D)^{1/2}$]. As shown in Figure 4, the combined parameters, $(V_{\rm r}D)^{1/2}$ and $V_{\rm r}\gamma$, have higher correlation coefficients [cc] with the Dst index than the other parameters [$V_{\rm p}$ and $V_{\rm r}$]: cc = 0.76 for $(V_{\rm r}D)^{1/2}$, cc = 0.70 for $V_{\rm r}\gamma$, cc = 0.55 for $V_{\rm r}$, and cc = 0.17 for $V_{\rm p}$. Our results are consistent with previous ones. Michalek *et al.* (2006) obtained a similar statistical trend: that $V_{\rm r}$ has a higher correlation coefficient with the Dst index than $V_{\rm p}$, and Michalek, Gopalswamy, and Yashiro (2007) showed that the combined parameter [$V_{\rm r}\gamma$] is better correlated with the Dst index. We find that $(V_{\rm r}D)^{1/2}$ and $V_{\rm r}\gamma$ are a little more sensitive to their Dst index than the other parameters ($V_{\rm p}$ and $V_{\rm r}$). These results imply that cone-model parameters together with the earthward-direction parameter improve the relationship between CME parameters and Dst index.

Table 1 Front-side full-halo CMEs (2001 – 2002).

Date	V_p [km s^{-1}]	Normalized V_p	D	V_r [km s^{-1}]	Normalized V_r	γ [deg]	Normalized γ	Source location	M	Dst [nT]
20 Jan 2001a	839	0.35	0.45	893	0.3	57	0.66	S07E40	N	−61
20 Jan 2001b	1507	0.63	0.3	1513	0.5	47	0.54	S07E46	S	−61
28 Jan 2001	916	0.38	0.32	1080	0.36	39	0.45	S04W59	S	−40
10 Feb 2001	956	0.4	0.41	1090	0.36	75	0.86	N37W03	N	−50
11 Feb 2001	1183	0.49	0.33	1150	0.38	62	0.71	N24W57	S	−50
19 Mar 2001	389	0.16	0.79	700	0.23	81	0.93	S20W00	S	−75
24 Mar 2001	906	0.38	0.74	1088	0.36	70	0.8	N15E22	S	−56
25 Mar 2001	677	0.28	0.57	1070	0.36	70	0.8	N16E25	N	−87
29 Mar 2001	942	0.39	0.94	2731	0.91	87	1.0	N20W19	S	−387
05 Apr 2001	1390	0.58	0.44	1360	0.45	58	0.67	S24E50	S	−59
06 Apr 2001	1270	0.53	0.65	1243	0.41	75	0.86	S21E31	S	−63
09 Apr 2001	1192	0.49	0.69	1549	0.51	77	0.89	S21W04	S	−271
10 Apr 2001	2411	1.0	0.49	2680	0.89	77	0.89	S23W09	S	−271
11 Apr 2001	1103	0.46	0.61	1423	0.47	72	0.83	S22W27	S	−77
12 Apr 2001	1184	0.49	0.5	1610	0.53	73	0.84	S19W43	S	−75
26 Apr 2001	1006	0.42	0.3	1396	0.46	76	0.87	N20W05	S	−47
14 Aug 2001	618	0.26	0.5	1042	0.35	84	0.97	N16W36	N	−105
24 Sep 2001	2402	0.99	0.37	3010	1.0	71	0.82	S16E23	S	−102
28 Sep 2001	846	0.35	0.69	1293	0.43	82	0.94	N10E18	S	−148
01 Oct 2001	1405	0.58	0.37	1415	0.47	49	0.56	S24W81	S	−166
09 Oct 2001	973	0.4	0.53	1116	0.37	65	0.75	S28E08	N	−71
19 Oct 2001	901	0.37	0.62	1465	0.49	83	0.95	N15W29	N	−187
22 Oct 2001	1336	0.55	0.43	2180	0.72	80	0.92	S21E18	S	−57
25 Oct 2001	1092	0.45	0.42	1335	0.44	75	0.86	S16W21	S	−157
04 Nov 2001	1810	0.75	0.77	2530	0.84	82	0.94	N06W18	S	−292
17 Nov 2001	1379	0.57	0.24	1460	0.49	54	0.62	S13E42	S	−48
22 Nov 2001a	1443	0.6	0.34	1683	0.56	70	0.8	S25W67	S	−221
22 Nov 2001b	1437	0.6	0.6	1833	0.61	73	0.84	S17W36	S	−221
13 Dec 2001	864	0.36	0.4	910	0.3	76	0.87	N16E09	N	−39
14 Dec 2001	1506	0.62	0.33	1493	0.5	43	0.49	N07E86	S	−39
14 Mar 2002	907	0.38	0.41	1000	0.33	65	0.75	S18E55	S	−37
15 Mar 2002	957	0.4	0.61	1030	0.34	79	0.91	S08W03	S	−37
22 Mar 2002	1750	0.73	0.47	1725	0.57	61	0.7	S10W90	S	−100
15 Apr 2002	720	0.3	0.86	1033	0.34	87	1.0	S15W01	S	−127
17 Apr 2002	1240	0.51	0.49	1720	0.57	76	0.87	S15W34	S	−149
21 Apr 2002	2393	0.99	0.47	2381	0.79	56	0.64	S14W84	S	−57
07 May 2002	720	0.3	0.5	831	0.28	76	0.87	S10E25	N	−110
08 May 2002	614	0.25	0.67	961	0.32	83	0.95	S12W07	N	−110
16 May 2002	600	0.25	0.41	1022	0.34	77	0.89	S23E15	N	−58
22 May 2002	1557	0.65	0.49	1724	0.57	71	0.82	S22W53	N	−109
18 Jul 2002	1099	0.46	0.22	1110	0.37	66	0.76	N19W30	N	−38
20 Jul 2002	1941	0.81	0.34	1683	0.56	46	0.53	S13E90	S	−38

Table 1 (*Continued*)

Date	V_p [km s^{-1}]	Normalized V_p	D	V_r [km s^{-1}]	Normalized V_r	γ [deg]	Normalized γ	Source location	M	Dst [nT]
26 Jul 2002	818	0.34	0.41	846	0.28	65	0.75	S19E26	N	−18
16 Aug 2002	1585	0.66	0.41	1576	0.52	74	0.85	S14E20	S	−106
22 Aug 2002	998	0.41	0.43	1151	0.38	52	0.6	S07W62	N	−45
24 Aug 2002	1913	0.79	0.33	1890	0.63	48	0.55	S02W81	S	−45
05 Sep 2002	1748	0.73	0.24	2638	0.88	75	0.86	N09E28	S	−181
09 Nov 2002	1838	0.76	0.27	1673	0.56	63	0.72	S12W29	N	−43
24 Nov 2002	1077	0.45	0.61	1433	0.48	81	0.93	N20E35	N	−64
19 Dec 2002	1092	0.45	0.55	1155	0.38	72	0.83	N15W09	N	−75

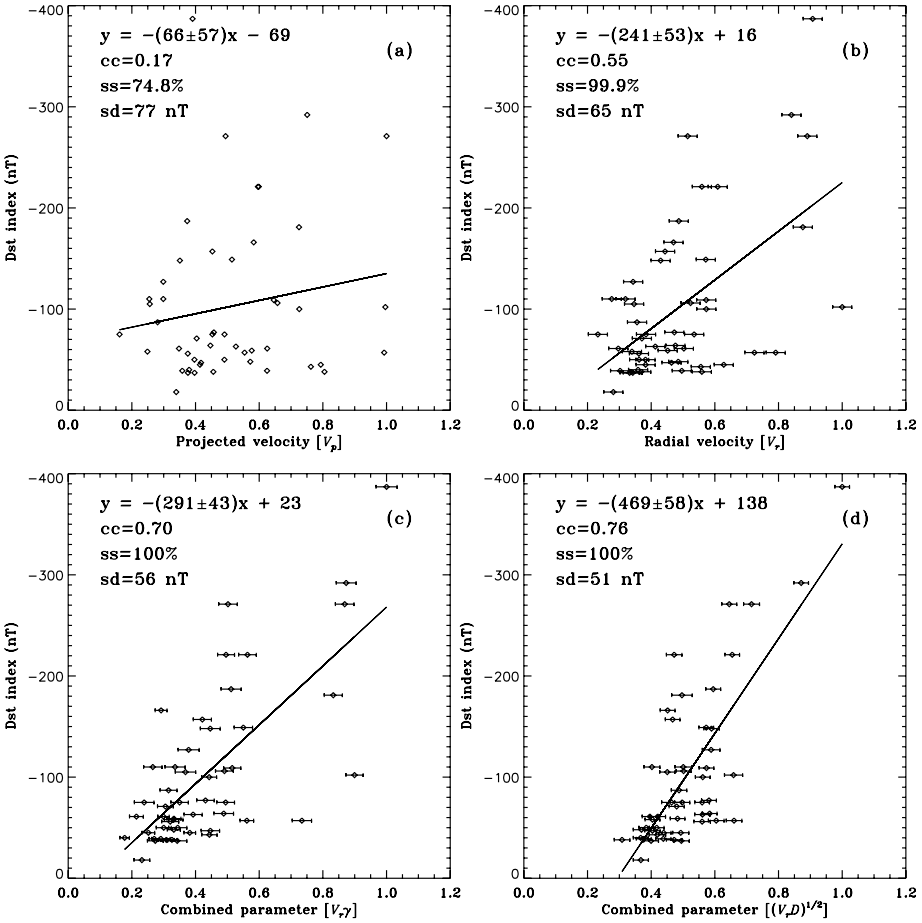

Figure 4 The relationship between CME parameters and the Dst index for four CME parameters: (a) projected velocity [V_p], (b) radial velocity [V_r], (c) combined parameter [$V_r\gamma$], (d) combined parameter [$(V_rD)^{1/2}$]. The solid line is a linear fit to all of the data points. The error bar of each parameter is determined by error-propagation analysis (Ku, 1966). cc, ss, and sd indicate correlation coefficient, statistical significance, and standard deviation, respectively.

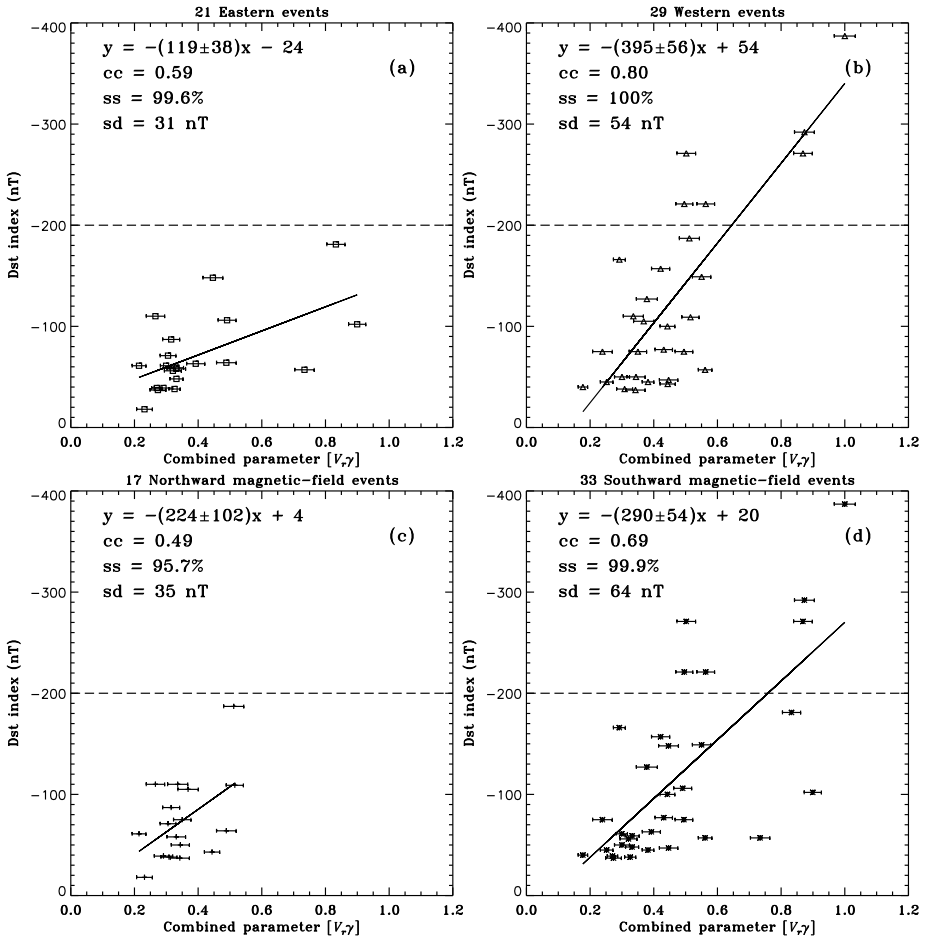

Figure 5 The relationship between the combined parameter $[V_{\mathrm{r}}\gamma]$ and the Dst index for four sub-groups according to their source longitudes and their magnetic-field orientations: (a) eastern events, (b) western events, (c) northward magnetic-field events, (d) southward magnetic-field events. The solid line is a linear fit to all of the data points. The horizontal broken line represents a Dst index of -200 nT. The error bar of each parameter is determined by error-propagation analysis. cc, ss, and sd indicate correlation coefficient, statistical significance, and standard deviation, respectively.

3.2. Dependence on Source Longitude and Magnetic-Field Orientation

To examine the dependence of the Dst index of the geomagnetic storms on the source longitudes of the 50 associated FFH CMEs, we divide the CMEs into two sub-groups: eastern events [E] and western events [W]. Figures 5a and b show the relationship between the combined parameter $[V_{\mathrm{r}}\gamma]$ and the Dst index of eastern and western events, respectively. For the eastern events the correlation coefficient, statistical significance, and standard deviation are 0.59, 99.6 %, and 31 nT, respectively (Figure 5a). Here the statistical significance is defined as $(1 - p\text{-value}) \times 100$. The p-value, which is the probability to accept the null hypothesis that both quantities are randomly distributed, is estimated by using the number of data and the correlation coefficient under the assumption of Student's t cumulative-distribution

function (Neter *et al.*, 1996). For the western events the correlation coefficient, statistical significance, and standard deviation are 0.80, 100 %, and 54 nT, respectively (Figure 5b). We find that western events have a higher correlation with the Dst index than eastern events, and super geomagnetic storms (Dst ≤ -200 nT) were only located in the western events, which is similar to the results of Michalek, Gopalswamy, and Yashiro (2007). In this study, we note that the slope of the western events is about three times larger than that of the eastern events, implying that FFH CMEs originating from the western region are more geoeffective than those from the eastern region.

To investigate the dependence of the Dst index of the geomagnetic storms on the magnetic-field orientations of the 50 associated FFH CMEs, we divide the CMEs into two sub-groups: northward magnetic-field events [N] and southward magnetic-field events [S]. Figures 5c and d show the relationship between the combined parameter $[V_{\rm r}\gamma]$ and the Dst index of northward magnetic-field and southward magnetic-field events, respectively. For the northward magnetic-field events, the correlation coefficient, statistical significance, and standard deviation are 0.49, 95.6 %, and 34 nT, respectively (Figure 5c). For the southward magnetic-field events, the correlation coefficient, statistical significance, and standard deviation are 0.69, 99.9 %, and 64 nT, respectively (Figure 5d). The correlations of southward events are quite similar to that of all events, but the correlations of northward events are smaller. This seems to be because the $V_{\rm r}\gamma$ and Dst values of northward events are much more confined than those of all events. Super geomagnetic storms (Dst ≤ -200 nT) only appear in the southward magnetic-field events. We find that the slope of the southward magnetic-field events is a little steeper than that of the northward magnetic-field events. Since the difference between the slopes of the northward and southward magnetic-field events is within the errors of the slopes, it is necessary to make a further study using more events.

Figure 6 shows the relationship between the combined parameter $[(V_{\rm r}D)^{1/2}]$ and the Dst index for four sub-groups according to their source longitudes and their magnetic-field orientations: (a) eastern events, (b) western events, (c) northward magnetic-field events, and (d) southward magnetic-field events. As shown in Figure 6,

i) super geomagnetic storms (Dst ≤ -200 nT) only appear in both the western and the southward magnetic-field events, and
ii) the slope of the western events is steeper than that of the eastern events.

These tendencies are consistent with the results of the relationship between the combined parameter $[V_{\rm r}\gamma]$ and the Dst index. Regarding the dependence of the Dst index on the magnetic-field orientations, we find that the slope of the southward magnetic-field events is a little steeper than that of the northward magnetic-field events. This tendency is more noticeable for $(V_{\rm r}D)^{1/2}$ than $V_{\rm r}\gamma$, which may imply that the earthward-direction parameter $[D]$ should be a better proxy for the direction than the angle between cone axis and sky plane $[\gamma]$ obtained by the asymmetric-cone model.

From Figures 4 – 6, we can find that linear-fitting relations have non-zero y-intercepts. This may imply that CMEs have certain values of $V_{\rm r}$ and D if they produce geomagnetic disturbances. For example, in Figure 6b, the linear-regression equation is Dst $= -507(V_{\rm r}D)^{1/2} + 148$. This means that when $(V_{\rm r}D)^{1/2}$ is larger than 0.48, the CME can produce intense geomagnetic storms (Dst ≤ -100 nT). It is noted that there is no CME with $V_{\rm r}D = 0$.

As a next step, we divide the CMEs into four sub-groups according to both their source longitudes and their magnetic-field orientations: eastern and northward magnetic-field events [E + N], eastern and southward magnetic-field events [E + S], western and northward magnetic-field events [W + N], and western and southward magnetic-field events

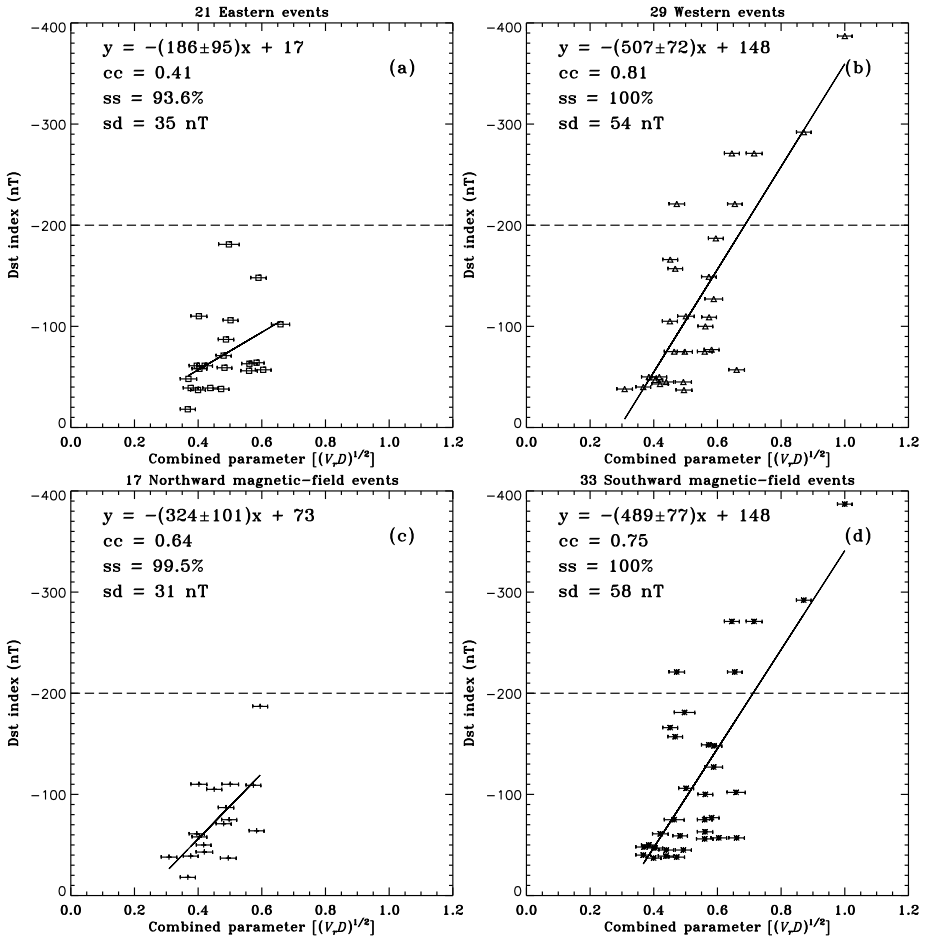

Figure 6 The relationship between the combined parameter $[(V_{\mathrm{r}}D)^{1/2}]$ and the Dst index for four sub–groups according to their source longitudes and their magnetic-field orientations: (a) eastern events, (b) western events, (c) northward magnetic-field events, (d) southward magnetic-field events. The solid line is a linear fit to all of the data points. The horizontal broken line represents a Dst index of -200 nT. The error bar of each parameter is determined by error-propagation analysis. cc, ss, and sd indicate correlation coefficient, statistical significance, and standard deviation, respectively.

[W + S]. Also, we examine the geomagnetic-storm fraction and mean Dst depending on the sub-group (Table 2). As can be seen in Table 2, one-third of the W + S events are super geomagnetic storms (Dst ≤ -200 nT) but all other sub-group events are moderate geomagnetic storms (-100 nT $<$ Dst ≤ -50 nT) or intense geomagnetic storms (-200 nT $<$ Dst ≤ -100 nT). That is, all super geomagnetic storms are found in the western and southward magnetic-field [W + S] events. Their mean absolute Dst values for geomagnetic storm events (Dst ≤ -50 nT) increase with the order of E + N, E + S, W + N, and W + S events. It is noted that the mean absolute Dst value (169 nT) of W + S events is significantly larger than that (75 nT) of E + N events. These results imply that we should consider source longitudes and magnetic-field orientations of CMEs to predict geomagnetic storms using CME parameters.

Table 2 Geomagnetic storm fraction and mean Dst depending on the sub-group.

	E + N	E + S	W + N	W + S
-100 nT $<$ Dst ≤ -50 nT	5/8	5/13	2/9	5/20
-200 nT $<$ Dst ≤ -100 nT	1/8	4/13	4/9	5/20
Dst ≤ -200 nT	0/8	0/13	0/9	6/20
Mean Dst [nT]	-75	-93	-106	-169
Standard deviations [nT]	18	43	26	100

4. Summary and Conclusion

In this study, we have investigated the relationship between CME parameters [V_p, V_r, $V_r\gamma$, and $(V_rD)^{1/2}$] and the Dst index as well as the dependence of geomagnetic storms on other CME parameters [L and M]. In addition, we have examined the geomagnetic-storm fraction and the mean Dst depending on sub-groups: E + N, E + S, W + N, and W + S. For this we used 50 FFH CMEs from 2001 to 2002 and their associated geomagnetic disturbances (Dst ≤ -18 nT).

The main results of this study can be summarized as follows: First, the combined parameters [$(V_rD)^{1/2}$ and $V_r\gamma$] have higher correlation coefficients [cc] with the Dst index than the other parameters [V_p and V_r]: cc = 0.76 for $(V_rD)^{1/2}$, cc = 0.70 for $V_r\gamma$, cc = 0.55 for V_r, and cc = 0.17 for V_p. Second, super geomagnetic storms (Dst ≤ -200 nT) only appear in the western and southward magnetic-field events. The mean absolute Dst values of geomagnetic storms (Dst ≤ -50 nT) increase in the order of E + N, E + S, W + N, and W + S events. These results confirm that the geoeffectiveness of FFH CMEs depends on their velocities, propagation directions, source longitudes, and magnetic-field orientations (Wang *et al.*, 2002; Moon *et al.*, 2005; Song *et al.*, 2006; Michalek, Gopalswamy, and Yashiro, 2007; Kim *et al.*, 2010). Our results demonstrate that not only the cone-model parameters together with the earthward-direction parameter improve the relationship between CME parameters and the Dst index, but also the longitude and the magnetic-field orientations of a FFH CME source region play a significant role in predicting geomagnetic storms.

Acknowledgements This work was supported by the BK21 plus program through the National Research Foundation (NRF) funded by the Ministry of Education of Korea, Basic Science Research Program through the NRF funded by the Ministry of Education (NRF-2013R1A1A2012763), NRF of Korea Grant funded by the Korean Government (NRF-2013M1A3A3A02042232), and the Korea Meteorological Administration/National Meteorological Satellite Center. R-SK has been supported by the Construction of Korean Space Weather Center as the project of KASI and Research Fellowship for Young Scientists of KRCF. The CME catalog is generated and maintained by the Center for Solar Physics and Space Weather, Catholic University of America, in cooperation with the Naval Research Laboratory and NASA. SOHO is a mission of international cooperation between the ESA and NASA. The Dst index is provided by the World Data Center for Geomagnetism at Kyoto University.

References

Abramenko, V.I.: 1986, *Glav. Astr. Obs.* **8**, 83. ADS:1986BsolD...8...83A.

Brueckner, G.E., Howard, R.A., Koomen, M.J., Korendyke, C.M., Michels, D.J., Moses, J.D., Socker, D.G., Dere, K.P., Lamy, P.L., Llebaria, A., Bout, M.V., Schwenn, R., Simnett, G.M., Bedford, D.K., Eyles, C.J.: 1995, *Solar Phys.* **162**, 357. doi:10.1007/BF00733434, ADS:1995SoPh..162..357B.

Brueckner, G.E., Delaboudinière, J.-P., Howard, R.A., Paswaters, S.E., St. Cyr, O.C., Schwenn, R., Lamy, P., Simnett, G.M., Thompson, B., Wang, D.: 1998, *Geophys. Res. Lett.* **25**, 3019. doi:10.1029/98GL00704, ADS:1998GeoRL..25.3019B.

Delaboudinière, J.-P., Artzner, G.E., Brunaud, J., Gabriel, A.H., Hochedez, J.F., Millier, F., Song, X.Y., Au, B., Dere, K.P., Howard, R.A., Kreplin, R., Michels, D.J., Moses, J.D., Defise, J.M., Jamar, C., Rochus, P., Chauvineau, J.P., Marioge, J.P., Catura, R.C., Lemen, J.R., Shing, L., Stern, R.A., Gurman, J.B., Neupert, W.M., Maucherat, A., Clette, F., Cugnon, P., Van Dessel, E.L.: 1995, *Solar Phys.* **162**, 291. doi:10.1007/BF00733432, ADS:1995SoPh..162..291D.

Gonzalez, W.D., Joselyn, J.A., Kamide, Y., Kroehl, H.W., Rostoker, G., Tsurutani, B.T., Vasyliunas, V.M.: 1994, *J. Geophys. Res.* **99**, 5771. doi:10.1029/93JA02867, ADS:1994JGR....99.5771G.

Gopalswamy, N., Yashiro, S., Akiyama, S.: 2007, *J. Geophys. Res.* **112**, A06112. doi:10.1029/2006JA012149, ADS:2007JGRA..112.6112G.

Gosling, J.T., McComas, D.J., Phillips, J.L., Bame, S.J.: 1991, *J. Geophys. Res.* **96**, 7839. doi:10.1029/91JA00316, ADS:1991JGR....96.7831G.

Kang, S.-M., Moon, Y.-J., Cho, K.-S., Kim, Y.-H., Park, Y.D., Baek, J.-H., Chang, H.-Y.: 2006, *J. Geophys. Res.* **111**, A05102. doi:10.1029/2005JA011445, ADS:2006JGRA..111.5102K.

Kim, R.-S., Cho, K.-S., Moon, Y.-J., Kim, Y.-H., Yi, Y., Dryer, M., Bong, S.-C., Park, Y.D.: 2005, *J. Geophys. Res.* **110**, A11104. doi:10.1029/2005JA011218, ADS:2005JGRA..11011104K.

Kim, R.-S., Cho, K.-S., Kim, Y.-H., Park, Y.D., Moon, Y.-J., Yi, Y., Lee, J., Wang, H., Song, H., Dryer, M.: 2008, *Astrophys. J.* **677**, 1378. doi:10.1086/528928, ADS:2008ApJ...677.1378K.

Kim, R.-S., Cho, K.-S., Moon, Y.-J., Dryer, M., Lee, J., Yi, Y., Kim, Y.-H., Wang, H., Park, Y.D., Kim, Y.H.: 2010, *J. Geophys. Res.* **115**, A12108. doi:10.1029/2010JA015322, ADS:2010JGRA..11512108K.

Ku, H.H.: 1966, *J. Res. Natl. Bur. Stand.* **70C**, 262.

Michalek, G.: 2006, *Solar Phys.* **237**, 101. doi:10.1007/s11207-006-0075-8, ADS:2006SoPh..237..101M.

Michalek, G., Gopalswamy, N., Yashiro, S.: 2003, *Astrophys. J.* **584**, 472. doi:10.1086/345526, ADS:2003ApJ...584..472M.

Michalek, G., Gopalswamy, N., Yashiro, S.: 2007, *Solar Phys.* **246**, 399. doi:10.1007/s11207-007-9081-8, ADS:2007SoPh..246..399M.

Michalek, G., Gopalswamy, N., Lara, A., Yashiro, S.: 2006, *Space Weather* **4**, S10003. doi:10.1029/2005SW000218, ADS:2006SpWea...410003M.

Moon, Y.-J., Cho, K.-S., Dryer, M., Kim, Y.-H., Bong, S.-C., Chae, J., Park, Y.D.: 2005, *Astrophys. J.* **624**, 414. doi:10.1086/428880, ADS:2005ApJ...624..414M.

Neter, J., Kutner, M.H., Wasserman, W., Nachtsheim, C.: 1996, *Applied Linear Statistical Models*, 4th edn., McGraw-Hill/Irwin, New York.

Pevtsov, A.A., Canfield, R.C.: 2001, *J. Geophys. Res.* **106**, 25191. doi:10.1029/2000JA004018, ADS:2001JGR...10625191P.

Scherrer, P.H., Bogart, R.S., Bush, R.I., Hoeksema, J.T., Kosovichev, A.G., Schou, J., Rosenberg, W., Springer, L., Tarbell, T.D., Title, A., Wolfson, C.J., Zayer, I., MDI Engineering Team: 1995, *Solar Phys.* **162**, 129. doi:10.1007/BF00733429, ADS:1995SoPh..162..129S.

Song, H., Yurchyshyn, V., Yang, G., Tan, C., Chen, W., Wang, H.: 2006, *Solar Phys.* **238**, 141. doi:10.1007/s11207-006-0164-8, ADS:2006SoPh..238..141S.

Srivastava, N., Venkatakrishnan, P.: 2004, *J. Geophys. Res.* **111**, A10103. doi:10.1029/2003JA010175, ADS:2004JGRA..10910103S.

Wang, Y.M., Ye, P.Z., Wang, S., Zhou, G.P., Wang, J.X.: 2002, *J. Geophys. Res.* **107**, 1340. doi:10.1029/2004JA010410, ADS:2004JGRA..109.9101Z.

Zhang, J., Dere, K.P., Howard, R.A., Bothmer, V.: 2003, *Astrophys. J.* **582**, 520. doi:10.1086/344611, ADS:2003ApJ...582..520Z.

Zhang, J., Richardson, I.G., Webb, D.F., Gopalswamy, N., Huttunen, E., Kasper, J.C., Nitta, N.V., Poomvises, W., Thompson, B.J., Wu, C.-C., Yashiro, S.: 2007, *J. Geophys. Res.* **112**, A10102. doi:10.1029/2007JA012321, ADS:2007JGRA..11210102Z.

Zhao, X.P., Webb, D.F.: 2003, *J. Geophys. Res.* **108**, 1234. doi:10.1029/2002JA009606, ADS:2003JGRA..108.1234Z.